CARDIFF UNIVERSITY
PRIFYSGOL CAERDYD

ORCA – Online Research @ Cardiff

This is an Open Access document downloaded from ORCA, Cardiff University's institutional repository:https://orca.cardiff.ac.uk/id/eprint/121821/

This is the author's version of a work that was submitted to / accepted for publication.

Citation for final published version:

Aswendt, Mark, Vogel, Stefanie, Schafer, Cordula, Jathoul, Amit , Pule, Martin and Hoehn, Mathias 2019. Quantitative in vivo dual-color bioluminescence imaging in the mouse brain. Neurophotonics 6 (2) , 025006. 10.1117/1.NPh.6.2.025006

Publishers page: http://dx.doi.org/10.1117/1.NPh.6.2.025006

Please note:
Changes made as a result of publishing processes such as copy-editing, formatting and page numbers may not be reflected in this version. For the definitive version of this publication, please refer to the published source. You are advised to consult the publisher's version if you wish to cite this paper.

This version is being made available in accordance with publisher policies. See http://orca.cf.ac.uk/policies.html for usage policies. Copyright and moral rights for publications made available in ORCA are retained by the copyright holders.

1
2
3
4
5 # Quantitative in vivo dual-color bioluminescence imaging
6 # in the mouse brain
7
8
9
10
11 Markus Aswendt[1,2,*], Stefanie Vogel[1], Cordula Schäfer[1], Amit Jathoul[3], Martin Pule[4],
12 Mathias Hoehn[1,5]
13
14
15
16 [1] In-vivo-NMR Laboratory, Max Planck Institute for Metabolism Research, Cologne, Germany
17 [2] University of Cologne, Faculty of Medicine and University Hospital Cologne, Department of
18 Neurology
19 [3] Molecular Biosciences, Cardiff School of Biosciences, Cardiff, UK
20 [4] Department of Haematology, Cancer Institute, University College London, London, UK
21 [5] Department of Radiology, Leiden University Medical Center, Leiden, Netherlands
22
23
24
25
26
27
28
29
30
31
32
33
34
35
36 ***Corresponding author:**
37 Markus Aswendt, PhD
38 University Hospital Cologne
39 Department of Neurology
40 Kerpener Strasse 62
41 50937 Cologne
42 Germany
43 +49 221 478-86416
44 markus.aswendt@uk-koeln.de

45

Abstract

Bioluminescence imaging (BLI) is an optical imaging method which can be translated from the cell culture dish in vitro to cell tracking in small animal models in vivo. In contrast to the more widely used fluorescence imaging which requires light excitation, in BLI the light is exclusively generated by the enzyme luciferase. The luciferase gene can be engineered to target and monitor almost every cell and biological process quantitatively in vitro and even from deep tissue in vivo. While initially used for tumor imaging, bioluminescence was recently optimized for mouse brain imaging of neural cells and monitoring of viability or differentiation of grafted stem cells. Here, we describe the use of bright color-shifted firefly luciferases (Fluc) based on the thermostable x5 Fluc that emit red and green for effective and quantitative unmixing of two human cell populations in vitro and after transplantation into the mouse brain in vivo. Spectral unmixing predicts the ratio of luciferases in vitro and a mixture of cells precisely for cortical grafts, however, with less accuracy for striatal grafts. This dual-color approach enables the simultaneous visualization and quantification of two cell populations on the whole brain scale with particular relevance for translational studies of neurological disorders providing information on stem cell survival and differentiation in one imaging session in vivo.

Keywords

spectral unmixing, luciferase, bioluminescence, stem cells, implantation, optical imaging

92 **Introduction**
93 Firefly luciferases (Flucs) are very efficient molecular and biochemical tools to track
94 cells, proteins, and to monitor gene expression in living organisms [1]. While the first
95 bioluminescence imaging (BLI) was limited to tumor applications [2], the firefly gene and
96 the detection hardware were continuously optimized to monitor other cell types, such as
97 stem cells and neurons, in deep tissue with higher or equal sensitivity and specificity
98 compared to for example fluorescence imaging [3–8]. BLI has some unique advantages
99 such as the light is produced directly in the Fluc expressing cells without the need of an
100 excitation source, promoting a very low background and high signal-to-noise ratios
101 (SNR). The efficiency of in vivo light production enables the detection of a minimal
102 number of 1,500 to 3,000 neural stem cells (NSCs) engrafted to the mouse brain,
103 through the intact skull, connecting tissue, and skin [9,10]. The survival rate of transplanted
104 cells, which is an important factor to determine the outcome of translational stem cell
105 studies, can be derived from the quantitative BLI signal, which requires adenosine
106 triphosphate (ATP) for the luciferase enzyme reaction [11]. Furthermore, the luciferase
107 gene was engineered to monitor the stem cell fate, for example the differentiation of
108 stem cells into early neurons in vivo [12]. However, these measurements can be
109 performed to-date only in separate, single color experiments. Multicolor BLI, the
110 simultaneous imaging of two or more luciferases with distinct emission spectra, emerged
111 first for in vitro assays and later for imaging bacteria or tumor cells in vivo [13–16]. Spectral
112 unmixing an algorithm that can distinguish the spectral signatures is applied to extract
113 the signal from two luciferases emitting light at different wavelengths and to calculates
114 the respective contribution of each reporter on every pixel of an image [16,17].
115 The aim of this study was to probe spectral unmixing for bioluminescence neuroimaging
116 with a focus on cell transplantation and to quantify the reliability of dual-color
117 measurements. We describe experiments with a bright red-shifted [18,19] and a novel
118 green-shifted point mutant of x5, a thermostable variant of wild type Fluc but with higher
119 quantum yields [20,21]. This dual-color pair was chosen based on a comparison to other
120 commonly used red/green Fluc mutants which showed efficient spectral unmixing in a
121 cell assay in vitro. Furthermore, we provide for the first time a quantitative in vivo
122 discrimination and unmixing-based estimation of two human neural stem cell populations
123 in the mouse brain. Such multiplexed bioluminescence approaches will be useful to
124 monitor the interaction of multiple cell populations in vivo and facilitate quantitative dual-
125 color neuroimaging.
126
127
128
129
130
131
132
133
134
135
136
137
138

139 **Results**
140

141 **In vitro spectral unmixing**

142 Previously described variations of wildtype (WT) firefly luciferase (Fluc) containing 5
143 mutations (F14R, L35Q, V182K, I232K, F465R)[22] that reduce surface hydrophobicity
144 and confer significant thermostability, were further mutated to red-shift (S284T) mutant
145 x5red (x5r)[18] and to produce a novel blue-shifted (V241I/G246A/F250S) mutant x5green
146 (x5g) bioluminescence spectra. In vitro, this novel dual-color Fluc pair was tested
147 against the bioluminescence spectra of WT Fluc (Promega, Madison, WI, USA),
148 PpyRE9 Fluc mutant [23], click beetle luciferase CBG99 [24], and Renilla luciferase hRluc [25]
149 were acquired with the IVIS Spectrum CT system equipped with 18 emission filter (20
150 nm bandpass) at 37°C. Each luciferase was expressed by transfection of lentiviral
151 vectors in the human tumor cell line HEK 293T. The bioluminescence signal was
152 corrected for the co-expressed copGFP fluorescence measured separately with a plate
153 reader. Here, copGFP levels reflect the transfection-based differences in luciferase
154 expression due to a specific viral T2A linker in the bicistronic lentiviral plasmid providing
155 equal expression levels of both transgenes. The normalized in vitro spectra [**Fig. 1**]
156 show differences in peak photon emission as well as spectra shape. Notably, x5g
157 produced in our setting the highest total photon flux (area under curve, AUC) compared
158 to CBG99 and Luc2 (1.79- and 3.69-fold, respectively). For x5r, we found the AUC value
159 to be 2.24-fold higher compared to PpyRE9 but only 0.45-times of the total photons from
160 Luc2. The photon flux from cells expressing hRluc cannot be compared directly due to
161 the different substrate (coelenterazine), however, the spectra clearly indicates the strong
162 monophasic blue/green light emission. In contrast, emission spectra of firefly and click
163 beetle luciferases follow a biphasic spline and in vitro/in vivo emission maxima of
164 520/560 nm (x5g, CBG99), 560/620 nm (PpyRE9, x5r) and 560/600 nm (Luc2). The
165 spectral separation is higher for x5g/x5r for all measured wavelengths compared to the
166 other green/red couples CBG99/PpyRE9, x5g/Luc2, and CBG99/Luc2. The second-best
167 separation is achieved by combining x5g and Luc2.
168 As the next step, we performed spectral unmixing of HEK 293T cells transfected with
169 x5g or x5r Fluc [**Fig. 2(a)**]. With the automated spectral unmixing algorithm provided by
170 the IVIS software, the green and red emission spectra of x5g and x5r were extracted
171 [**Fig. 2(b)**] and used for prediction of the x5g/x5r ratio in different mixtures [**Fig. 2(c)**].
172 The quantitative analysis of the unmixing data revealed high accuracy of predicted x5g
173 ratios in relation to the actual number of plated x5g cells [**(Fig. 2(d)**]. A linear regression
174 analysis showed that for both spectra, the unmixed photon counts are in linear
175 relationship to the amount of Fluc cells for both reporters, x5g and x5r (R^2=0.991
176 *p<0.001* and R^2=0.994, *p<0.001*). For the predicting the correct x5g/r ratios, the
177 algorithm results in a very low mean average deviation (MAD) of 0.02±0.02.
178

179 The influence of light absorption and scattering on the x5g/r Fluc photon emission was
180 determined with a tissue-like blood agar mix consisting of gelatine, intralipid, and
181 hemoglobin [**Fig. 3(a)**]. Plated x5g and x5r cells were covered with different amounts of
182 the blood agar mix before imaging in order to mimic cell grafts implanted at different
183 tissue depth. With increasing blood agar volume, the number of detected photons

184 decreased for x5r and x5g with an exponential two-phase decay [**Fig. 3(b)**]. The photon
185 flux of x5g compared to x5r remained on average 1.79-fold higher independent of blood
186 agar volume. Thus, under these in vitro conditions, no change in the x5g/r emission ratio
187 was detected and no additional correction factor for the Fluc-specific absorption was
188 calculated.

189 ## In vivo spectral unmixing

190 We determined the efficiency and accuracy of x5g and x5r Fluc unmixing in vivo by BLI
191 of transfected HEK 293T cells which were transplanted into nude mouse brains and
192 imaged on the following day. In comparison to other luciferases, x5g and x5r spectra
193 exhibit substantial differences [**Fig. 4**]. The normalized spectra of x5g reveals in
194 comparison to the green-shifted click beetle luciferase CBG99 at 560 nm a 2.07-fold
195 higher photon flux. Thus, the green shoulder of the x5g spectrum is much more
196 prominent. The differences between the two red-shifted firefly luciferases PpyRE9 and
197 x5r in terms of total photon flux and shape of the spectrum are much less distinct.
198
199 In order to identify the influence of transplantation depth, we performed experiments with
200 two separate groups: the cortical (-1.5 mm depth) as well as striatal (-3.0 mm depth)
201 grafts. The experimental setting [**Fig. 5(a, d)**] included mice with x5r and x5g cells only
202 as well as mice which received both cell types in in different mixtures. The two control
203 mice were used to extract the in vivo x5r and x5g spectra from the cortex and striatum
204 group in the auto unmixing mode, in which the software automatically detects x5r and
205 x5g [**Fig. 5(b, e)**]. Notably, the total photon flux of x5g and x5r luciferase in the cortex is
206 1.93-fold and 1.76-fold higher compared to the striatum. The emission maximum of x5r
207 is in both conditions at 620 nm but reached in the striatum only 58.44% photon flux of
208 the photon flux of cortical grafts. In case of x5g, the spectrum in the striatal group is 20
209 nm shifted and the maximal photon emission only 41.98% of the cortex group. In the
210 cortex group, automatic unmixing of the x5g ratio worked well with high accuracy for all
211 expected x5g ratios ($F(4,13)=217.455$, $p<0.001$). A general comparison of expected to
212 calculated x5g ratio resulted in a significant effect ($F(4,17)=79.961$, $p<0.001$), however,
213 with stronger linear correlation compared to the striatum ($R^2=0.994/p<0.001$ vs.
214 $R^2=0.933/p=0.008$) [**Fig. 5(c, f)**]. A post-hoc comparison showed that for example the
215 unmixing result is not precise enough to separate significantly cell grafts with 50 and
216 75% x5g cells, respectively ($p=0.179$). In order to further calculate the accuracy of
217 unmixing, the linear regressions for cortical and striatal grafts were statistically
218 compared to the implanted x5g ratios [Fig. 4(c, f)]. The difference between the slopes for
219 cortical and striatal grafts were not significantly different ($p=0.319$ and $p=0.450$). In
220 addition, a one sample t test was calculated to compare the unmixing results with the
221 known x5g ratio and the mean absolute deviation (MAD) was calculated to forecast the
222 error in an experiment. For cortical and striatal grafts all unmixing ratios were not
223 statistically significant different except of 100% x5g, which might be influenced by the
224 small variation and sample size. The MAD for cortical grafts was smaller (4.5) compared
225 to striatal grafts (8.0), supporting the observation that unmixing results and the expected
226 x5g ratios were found to be very reliable for the cortex and less reliable for the striatum
227 (**Table 1**).
228 We further processed the data assuming a scenario where the two control mice with x5g

and x5r cells for the auto unmixing mode are not present. The in vivo spectra and mean attenuation factors calculated from at 3 (cortex) or 4 (striatum) independent experiments were used to generate “library” spectra and to guide the unmixing algorithm [**Fig. 5(b, e)**]. In this case, the two control mice x5r and x5g would become obsolete. However, our calculations reveal less precise spectral unmixing for cortical and striatal grafts (**Table 1**). In the cortex group, statistically significant differences in x5g ratios were not predicted for 25 vs. 50 vs. 75% x5g cells in the mix. Most obvious is the strong under-representation of x5g in the mix especially for the striatal grafts which leads to false unmixing results, e.g. for 50% x5g in the striatum 23.0±4.1%, which is statistically significant different from the implanted 50% x5g cells. Similarly, the linear relationship for the increasing ratio of x5g cells in the mix holds true but with inferior correlation compared to the automated unmixing (cortex: $R^2=0.939/p=0.007$, striatum: $R^2=0.856/p=0.024$).

Table 1: Summary of in vivo unmixing validation.

	x5g%	Auto unmixing and pairwise comparison		One sample *t* test	MAD[1]	Library unmixing[2] and pairwise comparison		MAD[2]	One sample *t* test
Cortex	0	1.7±2.3		*p=0.239*	1.7	0.9±1.0		0.9	*p=0.120*
			] *p=0.035**				] *p=0.032**		
	25	21.5±9.9		*p=0.607*	8.8	20.9±9.3		8.3	*p=0.521*
			] *p=0.009***				] *p=0.189*		
	50	50.7±7.0		*p*=0.922	5.5	46.0±7.0		4.1	*p=0.270*
			] *p=0.016**				] *p=0.100*		
	75	65.0±4.1		*p*=0.078	7.3	54.1±8.2		20.9	*p=0.049**
			] *p=0.003***				] *p=0.002***		
	100	97.2±1.3		*p*=0.009**	3.3	90.8±6.1		9.2	*p=0.057*
Striatum	0	1.4±1.2		*p=0.052*	1.3	1.9±2.5		3.0	*p=0.203*
			] *p=0.005***				] *p=0.018**		
	25	18.0±8.1		*p=0.125*	10.0	7.9±2.9		14.7	*p=0.002***
			] *p=0.001****				] *p=0.003***		
	50	43.9±5.8		*p=0.211*	6.2	21.0±4.1		18.1	*p=0.005***
			] *p=0.170*				] *p=0.182*		
	75	55.7±16.5		*p=0.179*	19.3	28.1±13.2		31.6	*p=0.006***
			] *p=0.007***	*p=0.036**			] *p=0.005***		
	100	96.9±2.2			3.2	96.5±4.6		3.7	*p=0.095*

[2]Mean absolute deviation. [1]Calculated with mean attenuation factor calculated from auto unmixing experiments: cortex x5r/x5g (5.99±2.46/10.99±6.85), striatum x5r/x5g (9.04±4.02/11.50±7.51). Statistical significance reported as p-value result of the t-test between a pair adjacent x5g ratios.

Discriminating two different neural stem cell populations

In order to further probe the spectral unmixing approach, we tested x5g in combination with the widely used Fluc Luc2 in neural stem cells (NSCs). The human H9-NSC line was stably transduced using EF1α-Luc2-T2A-copGFP or DCX-x5g-T2A-EGFP lentiviral vectors and sorted by FACS for their GFP expression, respectively (data not shown).

252 The resulting two stable transgenic cell lines were transplanted into the cortex of nude
253 mice in the same mixture ratios as for the HEK 293T experiment (0/100, 25/75, 50/50,
254 and 100/0% x5g/r) and imaged one and two days later [**Fig. 6(a)**]. The quantitative
255 analysis revealed a linear correlation for both time points with a stronger correlation on
256 the first day after transplantation [**Fig. 6(b)**]. The presence of the different cell types was
257 verified by immunohistochemistry [**Fig. 6(c)**].

258 Discussion

259 We have recently characterized mutated luciferases originating from various species
260 such as *Photinus pyralis* Fluc (Luc2, PpyRE9), *Pyrophorus plagiopthalamus* (CBG99),
261 *Gaussia princeps* (Gluc), and *Renilla reniformis* (hRluc) for neuroimaging, which is
262 particularly challenging, as the bioluminescent photons need to pass thick layers of
263 bones and connective tissue. We further showed that spectral unmixing for CBG99 and
264 PpyRE9 is possible also for deep tissue grafts, however, with limitation to qualitative
265 analysis. [26] The aim of the present investigation was to optimize spectral unmixing for in
266 vivo bioluminescent neuroimaging by using advanced green- and red-shifted Fluc
267 mutants and characterize the accuracy to predict cell population ratios from quantitative
268 unmixing results.
269 The conventional in vitro dual-luciferase assay combines Renilla and firefly luciferases
270 [27]. These luciferases require different substrates (Fluc luciferin and Renilla
271 coelenterazine), which makes the bioluminescent signal distinguishable. However, for
272 many in vivo applications, the dual-luciferase approach is impractical because of the
273 weak quantum yield, the absorption- and scattering-sensitive blue light emitted by
274 Renilla, and it requires two separate imaging sessions. A different approach is spectral
275 unmixing, a dissecting algorithm, which is able to partition bioluminescence signals
276 originated from multiple fluorescence or luciferase sources into individual contributors
277 [16,28]. Although spectral unmixing is widely used in fluorescence microscopy for cell
278 imaging [29], in vivo applications - especially for neuroimaging - are technically
279 challenging. It requires sensitive BLI detectors and engineered luciferases with distinct in
280 vivo spectra. In a previous study, which was the first to compare reporter genes
281 specifically for mouse brain applications, we found the Fluc Luc2 to be superior to other
282 luciferases and the quantum yield (amount of photons emitted per luciferin molecule
283 processed) to be more important than emission wavelength [30]. As we have shown here,
284 tissue absorption and scattering have a significant impact on the luciferase spectrum,
285 making the in vivo spectrum considerably different from that in vitro.
286 For our comparison, we have used the previously described red-shifted x5 mutant[18,19,31]
287 and a novel green-shifted complement, x5g. They are based on a background that has
288 improved thermo-stability, solvent stability, pH-tolerance in terms of activity, and
289 resistance to bathochromic shift while retaining the same specific activity relative to the
290 wild type [18,23,31]. As we could show here, x5g and x5r have superior quantum yields and
291 a better spectral separation compared to the previously tested luciferases Luc2,
292 PpyRE9, CBG99, and hRluc [30]. The comparison of emission spectra from luciferases
293 expressed by HEK 293T cells in vitro and in vivo highlights the strong overlap of the
294 other green- and red-shifted luciferases with Luc2. The benefit of using x5g/x5r for
295 spectral unmixing compared to CBG99/PpyRE9 is a much stronger separation due to
296 higher photon flux and difference in spectrum shape. Especially under in vivo conditions,
297 the less pronounced attenuation of the green shoulder of x5g compared to CBG99

298 favors spectral separation also from deep tissue sources. Furthermore, the green-shifted
299 x5g is 1.79- and 3.69-fold brighter than CBG99 and Luc. Likewise, x5r is 2.24-fold
300 brighter than PpyRE9 [23,24] and the spectrum is characterized by a higher emission for
301 wavelengths above 600 nm. Red-shifted probes are considered to be more efficient in
302 vivo as light absorption in living tissue is negatively correlated with the emission
303 wavelength [24,32,33]. However, the lower quantum yield of red-shifted luciferases has so
304 far impeded sensitive detection of cell grafts in deep tissues, like the mouse brain [26].
305 The here tested x5r Fluc overcomes these limitations and was successfully validated for
306 in vitro and in vivo spectral unmixing applications.
307 Under in vitro conditions, the dual-luciferase pair x5r/g provided the best spectral
308 separation for all measured wavelengths compared to previously tested red and green-
309 emitting luciferases [26]. In this line, the unmixing of different ratios of transfected HEK
310 cells was straightforward with a minimal mean absolute deviation (MAD) of 0.02±0.02.
311 There was a highly significant linear correlation between cell number and (unmixed)
312 photon emission. In order to get reliable results, a simple correction factor compensating
313 for the individual filter attenuation must be applied. This filter attenuation is the relation
314 between the luciferase photon emission without filter vs. with filter and commonly used
315 for in vitro dual-color luciferase assays [34]. We imaged a tissue-like phantom with Fluc-
316 expressing cells covered with a blood and fat composition of human skin to model the in
317 vivo situation of transplanted cells in the living animal. Under these conditions, the
318 attenuation of photon emission due to increasing amounts of blood/fat follows an
319 exponential curve for both, x5g and x5r, while the difference in total photon emission
320 remains constant (x5g higher than x5r). According to that experiment, we did not
321 calculate an addition correction factor. However, the in vivo emission spectra from x5g-
322 and x5r-expressing HEK cells transplanted into the mouse brain revealed a strong tissue
323 depth-dependent difference compared to the in vitro cell culture and tissue model. Total
324 photon counts for x5g were much lower than for x5r. The total x5r photon counts were 5-
325 fold and 1.8-fold higher compared to x5g cells in the cortex and striatum, respectively.
326 The x5g peak emission was affected much stronger by tissue absorption compared to
327 x5r, which is in agreement with other in vivo mouse brain studies using for example the
328 red-shifted Fluc PRE9 [32]. Additional correction factors compensating for the Fluc-specific
329 tissue absorption as determined for subcutaneous tumors in mice [35] would be an
330 interesting target to further improve the quantification in future studies.
331 We found that the spectral unmixing algorithm works best when 2 “control” mice with x5g
332 and x5r engrafted cells were present to allow an automatic detection of “pure” light from
333 each luciferase. Although, the emission spectra were strongly influenced by tissue
334 absorption and scatter, statistical measures proved that for cortical grafts and with less
335 precision for striatal grafts quantitative unmixing is feasible. The mean absolute
336 deviation (MAD) for cells implanted in the cortex of adult mice was very low (4.5) and the
337 correlation of unmixing and actual x5g values followed a strict linear correlation which is
338 statistically not different, providing sufficient quantitative calculations of various mixtures
339 in dual-color imaging in vivo. In absence of both control mice, however, the automatic
340 unmixing algorithm tends to extract unrelated red and green components of the spectra
341 which may lead to wrong calculations of x5r/g ratio. The sampling of master spectra and
342 an average for the filter attenuation from a batch of independent experiments resolved
343 this problem only partially. In detail, we found less efficient unmixing for both, cortical
344 and striatal grafts under those conditions of using library data. While unmixing with the

345 generated library data (master spectra) predicts the ratio of x5g qualitatively good for
346 cortical grafts, it underestimates x5g in the striatal grafts. We speculate that the stronger
347 absorption of the green part of the spectrum negatively influences spectral unmixing
348 efficiency. Nevertheless, when sampled from more experiments, the library mode could
349 be useful for in vitro and ex vivo measurement, respectively, making controls and/or
350 additional animals with the pure green- and red-shifted luciferases obsolete.
351 Confounding factors for quantitative in vivo unmixing remain the biological variability in
352 luciferin distribution, reporter gene expression and the stability of the image acquisition.
353 Although the image acquisition was done in the steady-state of the luciferase activity (up
354 to 30 min post luciferin injection [9]), a random order of emission filters would prevent an
355 effect of lower/higher values related to the time after substrate injection. In order to
356 probe our spectral unmixing strategy in a more difficult application, we transduced
357 human NSCs with x5g and Luc2 constructs and transplanted different ratios into the
358 nude mouse brain. The dual-color luciferase pair x5g/Luc2 was chosen as quantum yield
359 and spectral separation are very similar to x5g/r. Furthermore, in this proof-of-concept
360 example, the widely used luciferase Luc2 is controlled by the constitutive human EF1α
361 promoter, which maintains Luc2 levels independent of NSC maturation state [12]. The x5g
362 expression is driven by the DCX promoter and provides a second readout specific for
363 early neurons. We could show that the dual-color luciferase approach is applicable to
364 human NSCs and that spectral unmixing of in vivo BLI early after stem cell
365 transplantation provides accurate and quantitative determination of undifferentiated vs.
366 pre-differentiated cells. In our experiments, the estimation of x5g ratios in the mix was as
367 good as for the HEK 293T cells at day 1 post implantation, but slightly worse the day
368 after. This might be due to different cell death behavior of the two cell lines or varying
369 DCX controlled reporter expression due to continuing neuronal differentiation. Due to
370 technical limitations, we have used two GFP reporter, copGFP and EGFP, for both
371 lentiviral vectors, which cannot be distinguished by fluorescence emission. In future
372 experiments it will be necessary to mirror the red/green luciferase also with a set of
373 equivalent fluorescent reporter to distinguish the cell types by histology. Notably, if a
374 direct correlation of GFP to Fluc expression is needed, a measurement of the actual
375 protein levels and the catalytic active protein, respectively, would be necessary [36]. The
376 T2A linker regulates bicistronic expression and not protein stability. Furthermore,
377 spectral unmixing should be tested with other improved pairs of luciferases and luciferins
378 such as AkaLumine-HCl[8] with enhanced sensitivity for deep tissue imaging. With these
379 technical improvements, imaging two different cell populations in the mouse brain at the
380 same time has many important applications. In stem cell therapy of neurological
381 disorders, for example, it could be used to monitor the viability and differentiation with
382 two different colored luciferases in order to answer the question if the stem cell graft
383 itself or an interplay of paracrine and immune-modulatory effects determine functional
384 improvement.

385 ## Conclusion

386 Here, we have shown that spectral unmixing of dual-color bioluminescence reporter can
387 determine the ratio of each luciferase. The unmixing was validated in human tumor and
388 neural stem cells engrafted into the mouse brain cortex. Monitoring the expression of the
389 two reporter genes by dual-color bioluminescence imaging holds great potential to
390 advance luciferase-based in vitro and in vivo assays. It enables simultaneous imaging of

391 protein and cell interaction in health vs. disease condition and holds the potential to
392 advance stem cell fate imaging.
393

394 **Material&Methods**

395 **Mutagenesis**

396 Thermostable x5 Fluc contains 5 mutations (F14R, L35Q, V182K, I232K, F465R) that
397 reduce surface hydrophobicity and confer significant thermostability[22]. The sequence of
398 human codon optimised WT Fluc was constructed by gene synthesis by oligo assembly
399 and the 5 mutations were added by splicing by overlap extension PCR-based cloning to
400 produce the plasmid MP5556x5, cloned into SFG-retrovirus[37] upstream an internal
401 ribosome entry site (IRES) and a truncated CD34 (dCD34) marker gene. Into this,
402 mutations were added to either produce blue-shifted (V241I/G246A/F250S) and red-
403 shifted (S284T) bioluminescence spectra in mutants x5green (x5g) and x5red (x5r),
404 respectively.

405 **Cell culture**

406 The human embryonic kidney cell line 293T (HEK 293T) was cultured in
407 DMEM+GlutaMAX medium (Life Technologies, Darmstadt, Germany) supplemented with
408 10% FBS (Life Technologies) and 1% Penicillin/Streptomycin (Life Technologies) under
409 humidified conditions at 37 °C and 5% CO_2. Cells were passaged every 3 days and
410 detached with Trypsin (Life Technologies). The human neural stem cell line H9-NSC
411 (Life Technologies), which were initially derived from the human embryonic stem cell line
412 H9 - NIH Registry WA09 [38] were maintained according to the manufacturer´s protocol.
413 Briefly, cells were plated on Geltrex coating at a density of $5x10^4$ cells/cm^2 in StemPro
414 NSC SFM complete medium consisting of 1x KnockOut DMEM/F-12, 2 mM GlutaMax,
415 20 ng/mL bFGF and EGF, and 2% StemPro supplement (Life Technologies). Cells were
416 passaged every 3 days and detached with StemPro Accutase (Life Technologies).

417 **Tissue-like phantoms**

418 Tissue-like phantom was prepared as follows: 8.76 mg/mL hemoglobin (Sigma-Aldrich)
419 and 40 mg/mL blood agar base (Sigma-Aldrich) were solved in 50 mM TBS buffer on a
420 hotplate stirrer at 50 °C. When both components were dissolved, Lipovenös MCT
421 (Fresenius Kabi, Bad Homburg, Germany) was added at a final concentration of 1%. For
422 the construction of the tissue phantom, the 96-well plate with the attached transfected
423 cells was placed on a 37 °C warming pad, the medium was removed, and the agar
424 mixture was layered carefully above the cells in various volumes ranging from 0 to 175
425 µL.

426 **Cell transfection and transduction**

427 HEK 293T cells were transfected with the plasmids pcDH-EF1α-x5g-T2A-
428 tdtomato+SV40Zeo or pcDH-EF1α-x5r-T2A-copGFP+SV40Zeo which consist of the
429 constitutive promoter elongation factor 1 alpha (EF1α), the genetically engineered x5
430 Fluc red (+S284T) [18,19,31] and the novel green (+ V241I/G246A/F250S) mutant, the self-
431 cleaving 2A-like peptide sequence from Thosea asigna virus (T2A), the green
432 fluorescent protein copGFP from Pontellina plumata (Exc 482nm, Em 502nm) or the red
433 fluorescent protein tdTomato (Exc 554nm, Em 581nm), the Simian virus 40 (SV40)
434 origin, and a Zeocin resistance gene (Zeo). Molecular cloning of plasmids carrying Luc2,

435 CBG99, PpyRE9, and hRluc was described previously [26]. For this study, we designed
436 novel bicistronic plasmids for constitutive and cell-specific expression of x5g and x5r by
437 amplifying recombinant DNA by PCR using specific primers bearing appropriate
438 restriction sites in the following steps. At first the backbone pcDH-EF1α-MCS-T2A-
439 copGFP (System Biosciences, Mountain View, USA) was changed to pCDH-EF1α-
440 MCS-T2A-tdTomato (pQC NLS TdTomato IX was a gift from Connie Cepko; Addgene
441 plasmid #37347). In addition, we added the antibiotic resistance gene zeocin controlled
442 by the independent SV40 promoter amplified from pBabe Zeo (pBABE zeo Ecotropic
443 Receptor was a gift from William Hahn, Addgene plasmid #10687). Secondly, x5g or x5r
444 were cloned with BamHI/NotI from M5556X5 or M5549X5 into pcDH-EF1α-MCS-T2A-
445 tdtomato+SV40Zeo or pcDH-EF1α-MCS-T2A-copGFP+SV40Zeo. For the cell specific
446 plasmids, fluorescence proteins were exchanged to tdTomato and EGFP (pmEGFP-1
447 was a gift from Benjamin Glick, Addgene plasmid #36409). The EF1α promoter was
448 exchanged by the human DCX promoter (kind gift of Sebastien Couillard-Despres,
449 Paracelsus Medical University, Salzburg, Austria) via ligation with the ClaI and XbaI
450 restriction sites. The final plasmids used for transduction of H9-NSCs were: pcDH-EF1α-
451 Luc2-T2A-copGFP and pcDH-DCX-x5green-T2A-EGFP. Successful cloning was verified
452 by restriction analysis and sequencing.
453 For transient transfection, HEK 293T cells were seeded (71,400 cells/cm^2) on gelatine
454 coated P60 cell culture dishes 12 h before transfection. Cells were transfected with 5.25
455 µg DNA and 10.5 µL Metafectene (Biontex, Munich, Germany) in 2 mL Opti-MEM
456 medium (Life Technologies) and incubated for 4 h under normal conditions. Post
457 transfection, cells were cultured for 2 to 3 days and prepared for in vitro dilution series or
458 in vivo implantation.
459 Lentiviral vector-mediated transduction of H9-NSCs was performed using 3rd generation
460 helper plasmids and subsequent cell incubation with unconcentrated pseudoviral
461 particles for 24 h (for experimental details see [12]). We selected stably expressing cell
462 lines based on the LTR-mediated background expression of EGFP and copGFP in the
463 transduced cells via FACS (FACSAria III, BD Biosciences, San Jos, USA).

464 Cell Transplantation

465 All experiments were conducted according to the guidelines laid out in the German
466 Animal Welfare Act and approved by the local authorities. Animals were kept in 12 h/12
467 h day/night cycle in individually ventilated cages. Food and water were offered ad
468 libitum.
469 Cells transplantation was performed as described before [9]. Transfected HEK 293T cells
470 were implanted individually or mixed (x5r:x5g; 1:1, 1:3 and 4:1) diluted with a final
471 concentration of 150,000 cells/µL in HBSS (Life Technologies) and stored on ice until
472 implantation. Cells were implanted into the right striatum (AP +0.5; L +2.0; DV −3.0
473 relative to bregma) or cortex (AP +0.5; L +2.0; DV −1.5 relative to bregma) of NMRI-
474 Foxn1nu/Foxn1nu mice (age 9-11 weeks, 25–30 g, male from Janvier, Saint Berthevin
475 Cedex, France). In total, we used 28 mice for cortical and 26 for striatal HEK 293T grafts
476 of which 6 and 3, respectively, were excluded because of visual bleeding out of the bore
477 hole.

478 In vitro and in vivo imaging set-up

479 Bioluminescence and fluorescence imaging experiments were performed with the IVIS
480 Spectrum CT (PerkinElmer, Waltham, USA). We recorded emission spectra explicitly
481 with the IVIS system as we used the system throughout all experiments and it was
482 shown by Zhao and colleagues previously that recording emission spectra with the IVIS
483 System results in comparable spectra acquired with a spectrophotometer [24].
484 For spectral unmixing of the in vitro dilution series respective cell numbers were diluted
485 in PBS (Life Technologies) and plated on a black clear bottom 96-well plate (Sigma-
486 Aldrich, Taufkirchen, Germany). D-luciferin potassium salt (Synchem, Felsberg,
487 Germany) was solved in PBS and added in a final concentration of 1 mM (~0.3 mg/mL).
488 Immediately after D-luciferin application, in vitro dilution series was imaged with
489 following settings: FOV 13.2 cm, Excitation Block, Emission 500 to 840 nm (20 nm
490 bandpass filter) and no filter (open filter setting), exposure time automatic, binning 8,
491 f/stop 1. In addition, copGFP fluorescence was measured using the plate reader
492 Mithras[2] LB943 (Berthold, Bad Wildbach, Germany) with the following settings:
493 Excitation 469 nm, Emission 510 nm, lamp energy 40%, counting time 2.0 sec. In vivo
494 BLI was performed one day post implantation. We used our mouse brain-adapted
495 imaging protocol, which was described in detail elsewhere [9]. 50 mg/mL D-luciferin
496 sodium salt (Synchem) was solved in PBS, sterile filtered, and injected intraperitoneally
497 to each animal with a final dose of 300 mg/kg body weight before Isoflurane (ISO)
498 anesthesia (2% ISO in 30% O_2/70% N_2O atmosphere). Image acquisition was started 8
499 min post D-luciferin injection for 25 min under following setting: FOV 22.5 cm, Excitation
500 Block, Emission 500 to 840 nm with 20 nm bandwidth and open filter. The exposure time
501 ranging from 1 to 60 sec, the lens aperture size, and the binning were set automatically
502 by the system to reach the most sensitive setting. Finally, animals were sacrificed and
503 brain tissues were processed for histology.

504 ## Immunostainings

505 For immunohistological staining of brain tissues, mice were transcardially perfused
506 under ISO anesthesia with 20 mL PBS followed by 20 mL 4% phosphate buffered
507 paraformaldehyde (PFA). Brains were removed and frozen in -40 °C cold 2-
508 methylbutane and stored at -80 °C. Brains were cut in 14 µm thick sections in coronal
509 plane with the cryostat (Leica, Wetzlar, Germany), mounted on object slides, and stored
510 at -20 °C. To equilibrate tissue, brain sections were washed 3 times with PBS. Antigen
511 retrieval was performed by incubating the brain sections in 10 mM sodium citrate buffer
512 (pH 6.0) at 80 °C for 30 min. Unspecific antibody binding was reduced by blocking with
513 5% normal donkey serum and 0.25% Triton X-100 in PBS for 1 h. Primary antibodies
514 were diluted with 0.25% Triton X-100 in PBS and incubated overnight at 4 °C. Brain
515 sections were stained for mouse anti-HuNu (Chemicon, 1:200) and rabbit anti-copGFP
516 (Evrogen, 1:200). Secondary antibodies – donkey anti-mouse-Cy5 (Jackson
517 Immunoresearch, 1:200) and donkey anti-rabbit-Cy3 (Jackson Immunoresearch, 1:200)
518 – were diluted with 0.25% Triton X-100 and Hoechst 33342 (Sigma-Aldrich, 1:000) in
519 PBS and incubated for 2 h. Finally, brain sections were air-dried and mounted within
520 Cytoseal XYL (Thermo Fisher Scientific).
521 All images were acquired with the BZ-9200 Microscope (Keyence, Neu-Isenburg,
522 Germany). Representative images of the immunohistological staining were acquired with
523 the 4x and 60x objectives and the respective phase contrast and fluorescence filter sets

524 (DAPI-BP, GFP-BP, TexRed, and Cy5 HC; Keyence).

525 Data analysis

526 Optical imaging data analysis and spectral unmixing was performed with the Living
527 Image 4.3.1 software (PerkinElmer). Regions of interest (ROIs) with constant size were
528 manually drawn for well plate quantification as well as in vivo data. Total photon flux was
529 calculated as area under curve as described previously [9] and the filter with highest
530 average radiance was selected as emission with maximum photon flux. The normalized
531 as well as non-normalized master spectrum for x5g and x5r in the striatum or cortex
532 were calculated by the average of 4 or 3 different acquisitions. The master spectrum
533 was used in the “library” mode for spectral unmixing as guideline. The automatic (“auto”)
534 spectral algorithm was used whenever possible, or replaced by the (manual) guided
535 unmixing in which the user has to pre-define where to find the pure x5g and x5r spectra.
536 The data for the unmixed populations of x5g and x5r were corrected for the experiment-
537 specific filter attenuation factor. This factor compensates for the difference between the
538 average radiance of x5g/r unmixing at a certain filter (usual 600-620/620-640 nm) and
539 the open filter (without filter) setting. Furthermore, this correction factor grades the
540 experimental variability induced by the differences during transfection and
541 transplantation. Without correcting for filter attenuation, the unmixing results will remain
542 qualitative. The filter attenuation factor average of all processed cortical and striatal
543 grafts was used for the master spectrum unmixing.
544 Histological images were processed with ImageJ 1.48s (National Institutes of Health,
545 Bethesda, USA). Further calculations, plotting, and statistical analysis were done with
546 MS-Excel 2010 (Microsoft Corporation, Redmond, USA) and SPSS 22.0 (IBM,
547 Ehningen, Germany). For multiple group comparisons the one-way ANOVA with Welch
548 statistics and post hoc pairwise comparison (Tukey-corrected) was used. A p-value ≤
549 0.05 was considered to be significant. A Student’s t-test was used for the comparison of
550 experimental groups. The one sample t-test was used to compare unmixing results with
551 the implanted x5g ratio. The mean absolute deviation (MAD) is the difference between
552 actual values and the known values (implanted x5g cells). All values are expressed as
553 mean ± standard deviation (SD) and statistical significance are indicated by $^*p<0.05$,
554 $^{**}p<0.01$, $^{***}p<0.001$., # n.s.

555

556
557
558

559
560
561
562
563
564
565
566

567

Biographies

568
569 **Markus Aswendt**, PhD, received his MSc degree in 2009 and PhD in neurobiology from
570 the University of Magdeburg and the Max Planck Institute in Cologne, Germany, in 2013
571 under Drs. Klaus Reymann und Mathias Hoehn. Following postdoctoral training in the
572 lab of Dr. Gary Steinberg, Stanford University School of Medicine, USA, he was
573 appointed a junior group leader in 2017 at the Department of Neurology, University of
574 Cologne. His lab explores neuroimaging in mice to develop therapies for stroke.
575
576 **Stefanie Vogel**, PhD, received here MSc degree and PhD in biology from the University
577 of Cologne, under Dr. Mathias Hoehn, Max Planck Institute for Metabolism Research,
578 Cologne, Germany in 2018. Currently, she is a postdoctoral fellow at the Technical
579 University Dresden, Germany, in the group of Dr. Jared Sterneckert.
580
581 **Cordula Schäfer**, is a technical assistant for molecular cloning and cell culture at the
582 Max Planck Institute for Metabolism Research, Cologne, Germany.
583
584 **Amit Jathoul**, PhD, received his PhD in biotechnology and chemical engineering at the
585 University of Cambridge, UK, in 2008. Following postdoctoral training with Martin Pule at
586 the University College London, UK, he became a research fellow in the School of
587 Biosciences at Cardiff University, UK, in 2016.
588
589 **Martin Pule**, PhD, received his Bachelor in Medicine and Surgery from the University
590 College in Dublin, Ireland, in 1995. Following a Fulbright Scholarship at the Baylor
591 College of Medicine, Houston, USA, he became a Senior Lecturer in Haematology at the
592 University of London Cancer Institute, London, UK. He leads the optical imaging in the
593 Center for Biological Imaging. He and his group work on engineering mammalian cells,
594 especially T-cells, for therapeutic applications.
595
596 **Mathias Hoehn**, PhD, received his MSC degree in 1978 and PhD in biophysics at the
597 University of Regensburg, Germany, in 1982. Following postdoctoral training at the
598 University of California, San Diego, USA, in 1984, he was appointed head of the MRI
599 group at the technical University of Aachen in 1985. Since 1987, he is leading the In-
600 vivo-NMR lab at the Max Planck Institute for Metabolism Research in Cologne, Germany
601 and was appointed a visiting professor in 2013 at the Leiden University Medical Center,
602 The Netherlands.

603

Disclosure

604 None.

605

Acknowledgments

606 We acknowledge excellent technical assistance with histology and in vivo imaging from
607 Anja Peglow and Andreas Beyrau. This work was financially supported by grants from
608 the EU-FP7 programs TargetBraIn (HEALTH-F2-2012-279017) and BrainPath (PIAPP-
609 GA-2013-612360). SV and MA were supported by a grant from the German research
610 foundation DFG (AS-464/1-1). AJ acknowledges the Welsh Government for a Ser

611 Cymru II Award (80762-CU-063).

612 ## References

613 1. C. E. Badr, Ed., *Bioluminescent Imaging*, Humana Press, Totowa, NJ (2014).
614 2. A. Rehemtulla et al., “Rapid and quantitative assessment of cancer treatment response
615 using in vivo bioluminescence imaging,” Neoplasia **2**(6), 491–495 (2000).
616 3. D.-E. Kim et al., “Imaging of stem cell recruitment to ischemic infarcts in a murine model,”
617 Stroke **35**(4), 952–957 (2004).
618 4. F. Sher et al., “Bioluminescence imaging of Olig2-neural stem cells reveals improved
619 engraftment in a demyelination mouse model,” Stem Cells **27**(7), 1582–1591 (2009).
620 5. A. Tennstaedt et al., “Noninvasive Multimodal Imaging of Stem Cell Transplants in the Brain
621 Using Bioluminescence Imaging and Magnetic Resonance Imaging,” in Methods in
622 Molecular Biology, pp. 153–166 (2013).
623 6. C. Vandeputte et al., “Bioluminescence imaging of stroke-induced endogenous neural stem
624 cell response,” Neurobiol. Dis. **69**, 144–155 (2014).
625 7. J. Adamczak et al., “Neurogenesis upregulation on the healthy hemisphere after stroke
626 enhances compensation for age-dependent decrease of basal neurogenesis,” Neurobiol.
627 Dis. **99**, 47–57 (2017).
628 8. S. Iwano et al., “Single-cell bioluminescence imaging of deep tissue in freely moving
629 animals,” Science **359**(6378), 935–939 (2018).
630 9. M. Aswendt et al., “Boosting bioluminescence neuroimaging: an optimized protocol for brain
631 studies,” PLoS One **8**(2), e55662 (2013).
632 10. S. Vogel et al., “Initial graft size and not the innate immune response limit survival of
633 engrafted neural stem cells,” J. Tissue Eng. Regen. Med. **12**(3), 784–793 (2018).
634 11. J. R. de Wet et al., “Firefly luciferase gene: structure and expression in mammalian cells,”
635 Mol. Cell. Biol. **7**(2), 725–737 (1987).
636 12. A. Tennstaedt et al., “Human neural stem cell intracerebral grafts show spontaneous early
637 neuronal differentiation after several weeks,” Biomaterials **44**, 143–154 (2015).
638 13. C. Daniel et al., “Dual-Color Bioluminescence Imaging for Simultaneous Monitoring of the
639 Intestinal Persistence of Lactobacillus plantarum and Lactococcus lactis in Living Mice,”
640 Appl. Environ. Microbiol. **81**(16), 5344–5349 (2015).
641 14. C. A. Maguire et al., “Triple bioluminescence imaging for in vivo monitoring of cellular
642 processes,” Mol. Ther. Nucleic Acids **2**, e99 (2013).
643 15. L. Mezzanotte et al., “A new multicolor bioluminescence imaging platform to investigate NF-
644 κB activity and apoptosis in human breast cancer cells,” PLoS One **9**(1), e85550 (2014).
645 16. S. T. Gammon et al., “Spectral unmixing of multicolored bioluminescence emitted from
646 heterogeneous biological sources,” Anal. Chem. **78**(5), 1520–1527 (2006).
647 17. S. K. Cool et al., “Comparison of in vivo optical systems for bioluminescence and
648 fluorescence imaging,” J. Fluoresc. **23**(5), 909–920 (2013).
649 18. B. R. Branchini et al., “Red- and green-emitting firefly luciferase mutants for bioluminescent
650 reporter applications,” Anal. Biochem. **345**(1), 140–148 (2005).
651 19. B. R. Branchini et al., “Thermostable red and green light-producing firefly luciferase mutants
652 for bioluminescent reporter applications,” Anal. Biochem. **361**(2), 253–262 (2007).
653 20. G. H. E. Law et al., “Mutagenesis of solvent-exposed amino acids inPhotinus
654 pyralisluciferase improves thermostability and pH-tolerance,” Biochem. J **397**(2), 305–312
655 (2006).
656 21. A. Jathoul et al., “Development of a pH-Tolerant Thermostable Photinus pyralis Luciferase
657 for Brighter In Vivo Imaging,” in Bioluminescence - Recent Advances in Oceanic
658 Measurements and Laboratory Applications, D. Lapota, Ed., InTech (2012).
659 22. G. H. E. Law et al., “Mutagenesis of solvent-exposed amino acids in Photinus pyralis

660 luciferase improves thermostability and pH-tolerance," Biochem. J **397**(2), 305–312 (2006).
661 23. B. R. Branchini et al., "Red-emitting luciferases for bioluminescence reporter and imaging
662 applications," Anal. Biochem. **396**(2), 290–297 (2010).
663 24. H. Zhao et al., "Emission spectra of bioluminescent reporters and interaction with
664 mammalian tissue determine the sensitivity of detection in vivo," J. Biomed. Opt. **10**(4),
665 41210 (2005).
666 25. S. Bhaumik and S. S. Gambhir, "Optical imaging of Renilla luciferase reporter gene
667 expression in living mice," Proceedings of the National Academy of Sciences **99**(1), 377–
668 382 (2001).
669 26. L. Mezzanotte et al., "Evaluating reporter genes of different luciferases for optimized in vivo
670 bioluminescence imaging of transplanted neural stem cells in the brain," Contrast Media
671 Mol. Imaging **8**(6), 505–513 (2013).
672 27. M. Hampf and M. Gossen, "A protocol for combined Photinus and Renilla luciferase
673 quantification compatible with protein assays," Anal. Biochem. **356**(1), 94–99 (2006).
674 28. C. Ran and A. Moore, "Spectral unmixing imaging of wavelength-responsive fluorescent
675 probes: an application for the real-time report of amyloid Beta species in Alzheimer's
676 disease," Mol. Imaging Biol. **14**(3), 293–300 (2012).
677 29. T. Zimmermann, "Spectral imaging and linear unmixing in light microscopy," Adv. Biochem.
678 Eng. Biotechnol. **95**, 245–265 (2005).
679 30. L. Mezzanotte et al., "Evaluating reporter genes of different luciferases for optimized in vivo
680 bioluminescence imaging of transplanted neural stem cells in the brain," Contrast Media
681 Mol. Imaging **8**(6), 505–513 (2013).
682 31. A. P. Jathoul et al., "A dual-color far-red to near-infrared firefly luciferin analogue designed
683 for multiparametric bioluminescence imaging," Angew. Chem. Int. Ed Engl. **53**(48), 13059–
684 13063 (2014).
685 32. Y. Liang, P. Walczak, and J. W. M. Bulte, "Comparison of red-shifted firefly luciferase Ppy
686 RE9 and conventional Luc2 as bioluminescence imaging reporter genes for in vivo imaging
687 of stem cells," J. Biomed. Opt. **17**(1), 016004 (2012).
688 33. L. Mezzanotte et al., "Sensitive dual color in vivo bioluminescence imaging using a new red
689 codon optimized firefly luciferase and a green click beetle luciferase," PLoS One **6**(4),
690 e19277 (2011).
691 34. E. Michelini et al., "Spectral-Resolved Gene Technology for Multiplexed Bioluminescence
692 and High-Content Screening," Anal. Chem. **80**(1), 260–267 (2008).
693 35. S. Pesnel et al., "Quantitation in bioluminescence imaging by correction of tissue absorption
694 for experimental oncology," Mol. Imaging Biol. **13**(4), 646–652 (2011).
695 36. K. A. Feeney et al., "In-depth Characterization of Firefly Luciferase as a Reporter of
696 Circadian Gene Expression in Mammalian Cells," J. Biol. Rhythms **31**(6), 540–550 (2016).
697 37. B. Philip et al., "A highly compact epitope-based marker/suicide gene for easier and safer T-
698 cell therapy," Blood **124**(8), 1277–1287 (2014).
699 38. S. K. Dhara and S. L. Stice, "Neural differentiation of human embryonic stem cells," J. Cell.
700 Biochem. **105**(3), 633–640 (2008).

701

702

703

704

705

706

707 ## Figure legends

708

709 **Fig. 1: Comparison of Luc2, CBG99, PpyRE9, x5g, x5r, and hRluc emission specra**
710 **in vitro.** Plotted is the photon emission from EF1α-luciferase-T2A-copGFP transfected
711 HEK 293T cells recorded with the IVIS Spectrum CT system (mean of n=4-6). Photon
712 emission was normalized to the individual copGFP expression. Graph with grey
713 background is a zoom-in for 580-700 nm to highlight differences in the red part of the
714 spectra.

715

716 **Fig. 2. Unmixing of x5g and x5r luciferases expressed by HEK 293T cells.** (a)
717 Fluorescence microscopy overlay with phase contrast image of cells at 2 days post
718 transfection, used for the unmixing experiment (scale bar 25 µm). (b) Unmixed spectra
719 of x5r and x5g calculated by the unmixing algorithm. (c) Plating scheme for x5g and x5r
720 cells in different numbers (n=3) and the corresponding false-colored unmixed result
721 displayed as green/red composite as well as the open filter, x5g, and x5 red unmixed
722 images. (d) Plot of measured unmixed x5g and x5r photon flux plotted vs. the plated
723 ratio of x5g cells in the mix (n=3). Linear fitting for both luciferases underlines high
724 accuracy of unmixed values with plated cells.

725

726 **Fig. 3: In vitro modeling of superficial vs. deep x5g and x5r Fluc sources with**
727 **tissue-like agarose.** (a) Different volumes of tissue-like agarose were placed above the
728 HEK 293T cell layer to mimic overlaying tissue in different thickness. Micrographs
729 represent selected bioluminescence/photo overlays from the x5g and x5r unmixing,
730 respectively. (b) Quantitative analysis and polynomial fit for the decreasing photon
731 emission, detected when more blood agar volume was added.

732

733 **Fig. 4:** In vivo emission spectra of x5g and x5r in comparison to Luc2, CBG99, PpyRE9,
734 and hRluc expressed in mammalian cells implanted in the mouse brain (data in part
735 adapted from our previous publication comparing different luciferases [26]).

736

737 **Fig. 5. Spectral unmixing efficiently determines x5g/r cell ratios in vivo.** Transiently
738 transfected HEK 293T cells expressing x5g or x5r luciferases were transplanted into the
739 cortex **(a)** or striatum **(d)** and bioluminescence imaging was applied 1 day later. Non-
740 normalized spectra from the x5g and x5r cells differ, dependent on transplantation
741 depth: cortex **(b)**, striatum **(e)**. Spectral unmixing of x5g ratio is in good agreement with
742 expected (dotted line) x5g ratio for the cortical **(c)** as well as striatal **(f)** grafts. Significant
743 differences are highlighted by asterisks.

744

745 **Fig. 6. Spectral unmixing of two neural stem cell (NSC) populations. (a)** NSC lines
746 expressing x5g or Luc2 were implanted in different ratios into the cortex of nude mice.
747 **(b)** Quantitative analysis of spectral unmixing from imaging data acquired 1 day and 2
748 days post implantation (dpi). **(c)** Representative immunohistochemical staining of an
749 NSC graft (EF1α-Luc2-T2A-copGFP). Human nuclei (HuNu) to discriminate the human
750 cell graft in the mouse brain. Enhanced copGFP with anti-copGFP antibody to visualize
751 transplanted cells expressing the transgene. Hoechst to visualize cell nuclei. Scale bar

752 50 um.
753

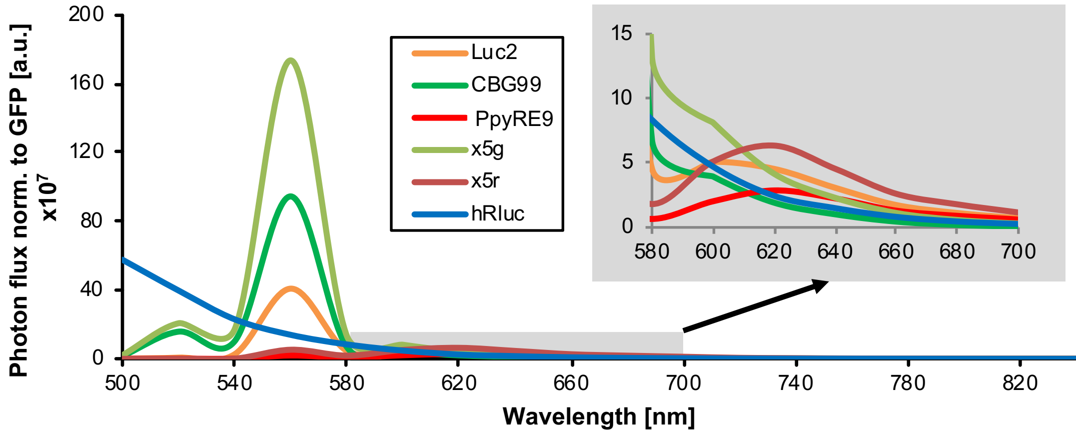
Photon flux norm. to GFP [a.u.] x10^7
Wavelength [nm]
200
160
120
80
40
0
500
540
580
620
660
700
740
780
820
Luc2
CBG99
PpyRE9
x5g
x5r
hRluc
15
10
5
0
580
600
620
640
660
680
700

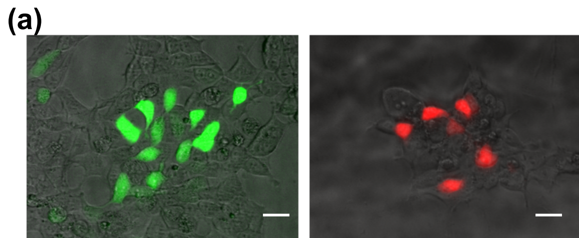
(a)

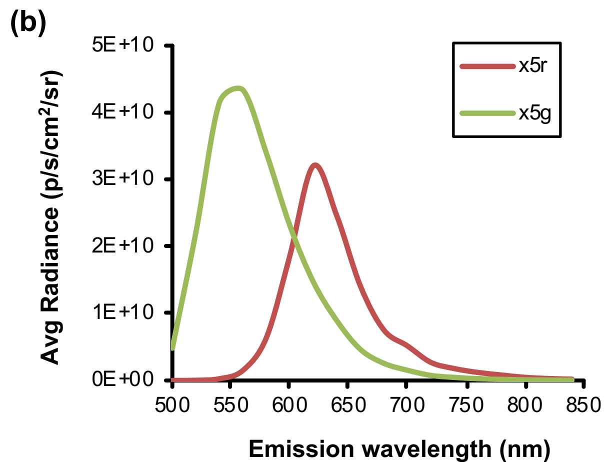
(b)
x5r
x5g
Avg Radiance (p/s/cm²/sr)
5E+10
4E+10
3E+10
2E+10
1E+10
0E+00
500
550
600
650
700
750
800
850
Emission wavelength (nm)

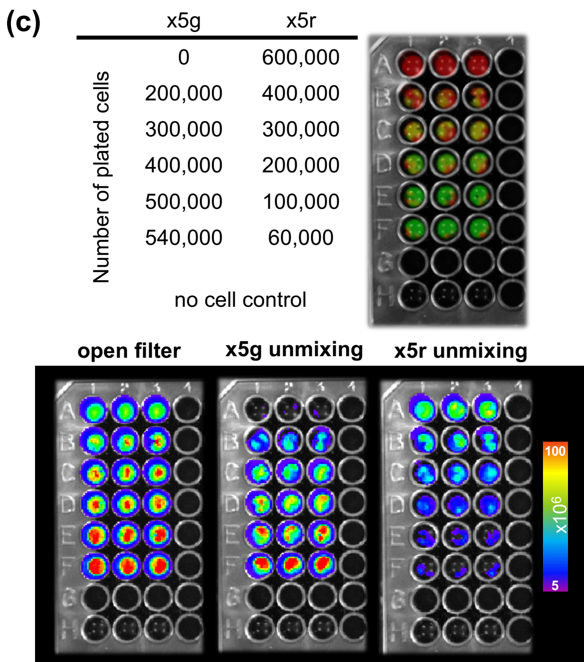
(c)
Number of plated cells
x5g
x5r
0
600,000
200,000
400,000
300,000
300,000
400,000
200,000
500,000
100,000
540,000
60,000
no cell control
open filter
x5g unmixing
x5r unmixing
100
x10⁶
5

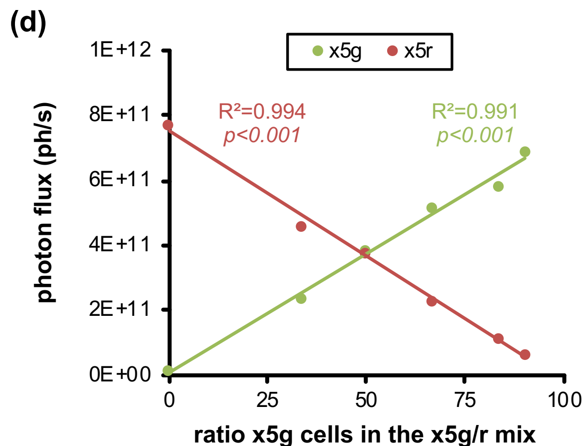
(d)
x5g
x5r
photon flux (ph/s)
1E+12
8E+11
6E+11
4E+11
2E+11
0E+00
R²=0.994
p<0.001
R²=0.991
p<0.001
0
25
50
75
100
ratio x5g cells in the x5g/r mix

(a)
agar
Fluc
x5g unmix
x5r unmix
0
x5g
x5r
25
x5g
x5r
75
x5g
x5r
125
x5g
x5r
175
x5g
x5r
50
x10^6
5
(b)
Avg Radiance [p/s/cm²/sr]
1E+08
9E+07
6E+07
3E+07
0E+00
x5g
x5r
R²=0.9386
R²=0.9884
**
**
**
**
*
0
50
100
150
200
Blood agar volume [ul]

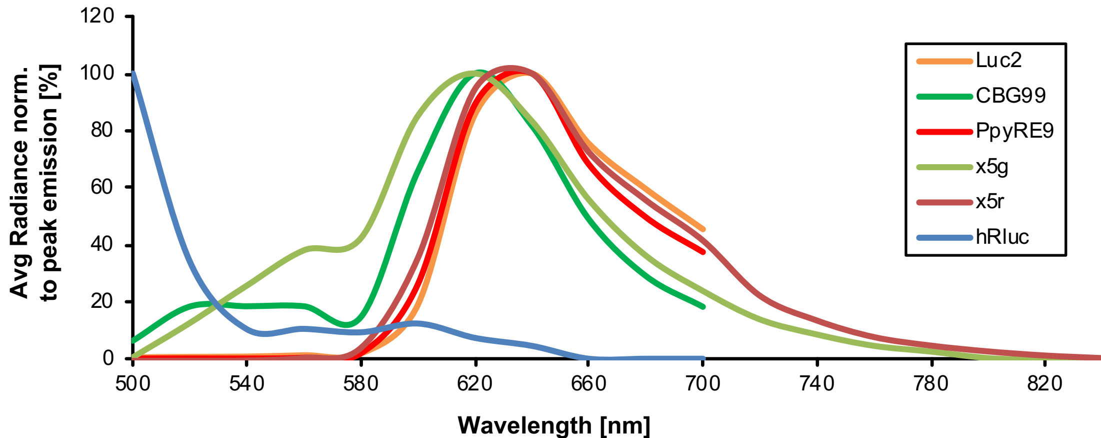
Avg Radiance norm. to peak emission [%]
120
100
80
60
40
20
0
500
540
580
620
660
700
740
780
820
Wavelength [nm]
Luc2
CBG99
PpyRE9
x5g
x5r
hRluc

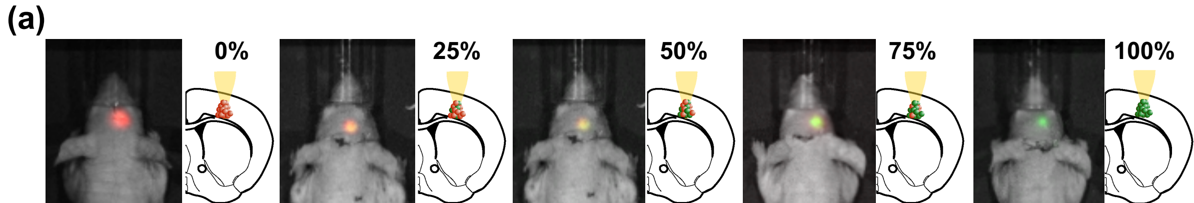
(a)
0%
25%
50%
75%
100%
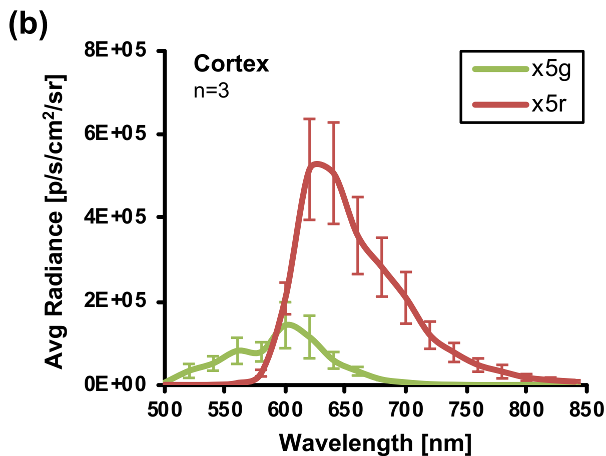
(b)
Cortex
n=3
x5g
x5r
Avg Radiance [p/s/cm²/sr]
8E+05
6E+05
4E+05
2E+05
0E+00
500
550
600
650
700
750
800
850
Wavelength [nm]
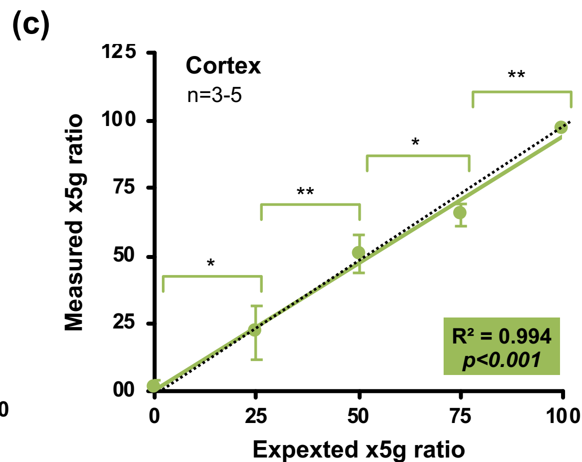
(c)
Cortex
n=3-5
Measured x5g ratio
125
100
75
50
25
00
0
25
50
75
100
Expexted x5g ratio
*
**
*
**
R² = 0.994
p<0.001
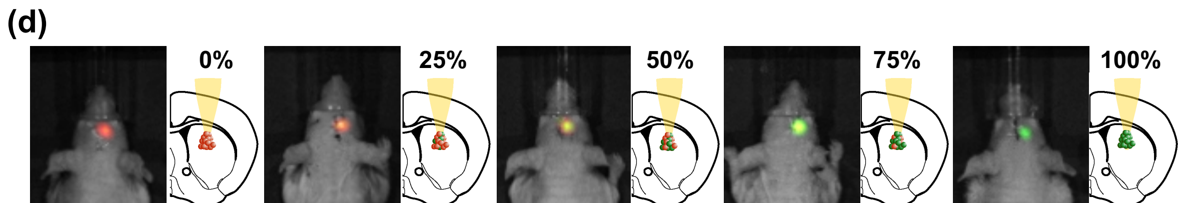
(d)
0%
25%
50%
75%
100%
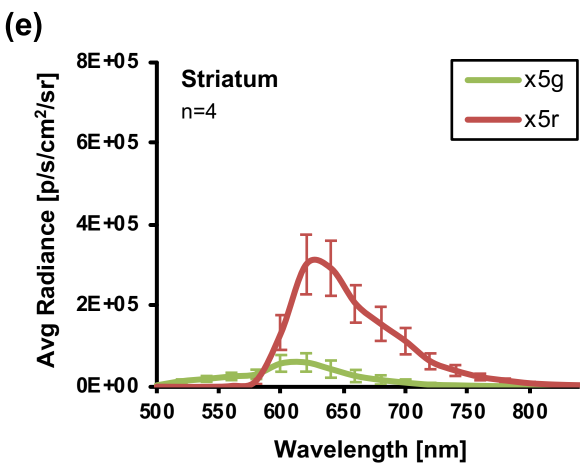
(e)
Striatum
n=4
x5g
x5r
Avg Radiance [p/s/cm²/sr]
8E+05
6E+05
4E+05
2E+05
0E+00
500
550
600
650
700
750
800
Wavelength [nm]
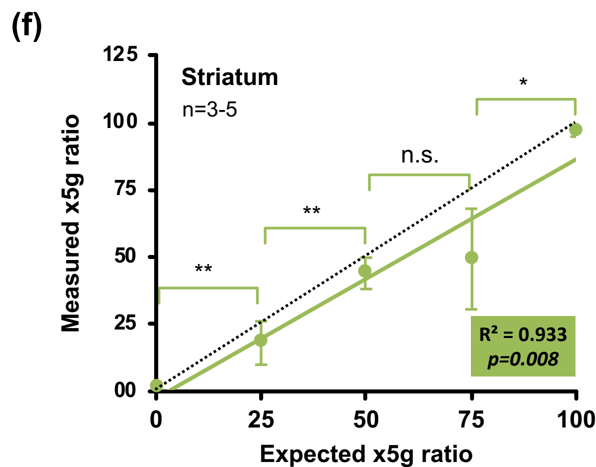
(f)
Striatum
n=3-5
Measured x5g ratio
125
100
75
50
25
00
0
25
50
75
100
Expected x5g ratio
**
**
n.s.
*
R² = 0.933
p=0.008

(a)

0% x5g
25% x5g
50% x5g
75% x5g
100% x5g

x5g unmixing

Luc2 unmixing

3.0
1.5
0
x10⁵ ph/s/cm²/sr